Available online at www.sciencedirect.com
SCIENCE DIRECT®
Journal of Sound and Vibration 288 (2005) 1077–1104
JOURNAL OF SOUND AND VIBRATION
www.elsevier.com/locate/jsvi

Control of tonal noise from subsonic axial fan. Part 2: active control simulations and experiments in free field

Anthony Gérard, Alain Berry*, Patrice Masson

G.A.U.S., Mechanical Engineering Department, Université de Sherbrooke, 2500 blvd Université, Sherbrooke, Que., Canada J1K 2R1

Received 20 January 2004; received in revised form 5 January 2005; accepted 23 January 2005
Available online 31 March 2005

Abstract

This paper deals with the global control of engine cooling fan noise in free field at the Blade Passing Frequency (BPF) and its first harmonic. The aim of this paper is to investigate the feasibility of using a single loudspeaker in front of the fan to cancel the tonal noise. A simplified model of fan noise, which only takes into account the most radiating circumferential mode of the forces acting by the fan on the fluid, is first combined with an unbaffled loudspeaker model to predict the residual sound field for various sensor configurations. Metrics for global control such as sound directivity or sound power attenuation reveal that the control is effective with this simplified model in the whole space at low frequency, depending on the number and location of the error sensors. However, for non-homogeneous flow, other circumferential modes may contribute to the sound radiation and then, the inverse model described in the companion paper is used to provide a more accurate extrapolated sound field from the reconstructed unsteady aerodynamic forces acting by the fan on the fluid. Simulation results demonstrate the global control in the downstream half space of the blade passing frequency and its first harmonic using a single error microphone and a single control source. A single-input–single-output (SISO) adaptive feedforward controller is implemented experimentally to drive the control loudspeaker. The tones at the BPF and at its first harmonic are attenuated by up to 28 and 18 dB, respectively at the far field error microphone.

*Corresponding author. Tel.: +1 819 821 8000x2148; fax: +1 819 821 7163.
E-mail address: alain.berry@usherbrooke.ca (A. Berry).

0022-460X/$ - see front matter © 2005 Elsevier Ltd. All rights reserved.
doi:10.1016/j.jsv.2005.01.022

Nomenclature

a	piston radius
a_1	inner rotor radius
a_2	outer rotor radius
B	number of blades
c	speed of sound
f	frequency
f_z	axial pressure component acting on the rotor
f_z^0	time average value of the axial pressure
F_t	total thrust of the propeller
g_{1z}	Green function (dipolar radiation along the z-axis)
i	imaginary number ($\sqrt{-1}$)
I	number of radial elements
J_p	cost function
J_{nb+q}	Bessel function of the $(nB+q)$th order
k	wavenumber ($k = sk_1 = s\omega_1/c$ with $\omega_1 = B\Omega$)
L	number of control point
p	acoustic pressure
q_p, q_s	complex source strength of the primary and secondary sources
$q_{\min}$, $q_{\max}$	minimum and maximum circumferential order q to be reconstructed
r, φ, ϑ	spherical coordinates in the radiation space
x, y, z	Cartesian coordinates in the radiation space
r_1, φ_1	polar coordinates in the rotor plane
$\bar{r}_1$	mean radius of the fan
t	time
W	total sound power
z_s	source separation
$\mathbf{z}$	complex acoustic transfer function
α_n	time Fourier coefficient
β_q	azimuthal Fourier coefficient
Δr_1	distance between two radial elements
η	sound pressure control parameter
η_W	sound power control parameter
η_W^{half}	half-space sound power parameter
λ	wavelength
ρ	mass density of air
ω	angular frequency
ω_1	blade passage angular frequency ($\omega_1 = B\Omega$)
Ω	angular velocity of the rotor

Subscripts and indices

l	control point index
p	primary source subscript
q	circumferential index
n	harmonic order of the BPF
s	secondary source subscript
i	radial element index
L	condensed source discretization index (i, q)
z	axial component subscript
φ	radial component subscript

Superscripts

H	Hermitian
T	vector transpose
*	complex conjugate

1. Introduction

Fan noise and aerodynamic noise are, in general, accounting for an increasing part of the total noise inside the cabin as motors are becoming quieter. A particular annoying source comes from the tonal noise of automotive axial engine cooling fans residing within a range from 100 to 700 Hz. For those frequencies, passive techniques are bulky, inefficient and cannot be applied to the automotive industry but active control techniques are better adapted to those frequencies and have a great potential for an "at the source" control.

Many investigators have focussed on the active control of low-frequency ducted fan noise (see for example Nelson and Elliot [2], Eriksson et al. [3], Yeung et al. [4]). These approaches are based

on a modal description of sound propagation in ducts (waveguides), which consider plane waves for frequencies with wavelengths at least twice the greatest dimension of the cross-section of the duct and which require a single loudspeaker to be actively cancel. For higher frequencies, a non-uniform acoustic pressure distribution associated with higher-order propagating modes appears. Efforts have been made to control both the low-frequency tonal noise and broadband noise. The active control techniques use either (1) an acoustic reference signal, where the system instability which may occur due to the feedback of the control signal to the reference microphone is prevented by modelling this feedback loop and subtracting it from the measured reference (internal model controller [3]) or (2) an optical sensor for periodic sources that eliminates this feedback constraint, which is appropriate for active tonal fan noise control. Erikson [3] for example reported attenuations of about 10 dB over the range 20–300 Hz. Passive/active hybrid noise control systems have also been studied to reduce both discrete and broadband noise. Kostek [5] developed a system combining fully active noise control with adaptive passive tunable Helmholtz resonators for ducted fan noise.

Recently, Wong [6] proposed a hybrid solution to control the exhaust fan noise of a computer room into a corridor. He used a short square duct with thick wool blanket that provides a passive system to attenuate broadband noise above 800 Hz, a decrease in the A-weighted overall sound pressure of 2 dB was obtained. Then, he combined it with an active control system for tonal noise attenuation using a loudspeaker mounted in the short duct to cancel the tonal noise up to 25 dB for the first blade passing frequency (BPF). This cannot be applied to the automotive engine cooling fan because of space constraints.

Recent works have also been conducted on the computer simulations on the active control of fan tones radiated from the intake of turbofans using an annular secondary source ring and in-duct error sensors or external error sensors [7]. Thomas et al. [8] applied a feedforward filtered-X LMS to an operational engine turbofan and obtained attenuations up to 12 dBA for the fundamental frequency and 5 dBA along the engine axis with reference transducers mounted on the engine case, providing BPFs information, far-field error microphones and annular secondary source ring (24 loudspeakers) mounted in the inlet.

A speaker dipole arrangement (up to 3) around each vane of a three-vane stator was investigated by Myers and Fleeter [9] to attenuate the propagating acoustic wave due to rotor–stator interaction by up to 15 dB in the upstream and 15.7 dB in the downstream for the circumferential mode -2. All the previously cited researches are based on an acoustical duct modal approach, principally aiming at reducing the blade passing frequencies tones but cannot directly apply to the automotive engine cooling fan case.

Other papers on turbofan noise consist in actively reducing the unsteady rotor/stator interaction. Rao et al. [10] demonstrated the control of the unsteady interactions between a stator and a rotor of a 1/14-scale turbofan by injecting wakes from the trailing edge of stator vanes using microvalves and consequently reduced the BPF tone in the whole measured space by up to 8.2 dB depending on the speed of the fan and the measurement direction, and the sound power level was reduced by up to 4.4 dB. The main advantage of this approach is the reduction of the circumferential variation velocity of the flow; it can therefore control the sound at the source but the spectrum presented in this paper does not show a complete cancellation of the discrete noise and is too expensive for an automotive application. Kousen and Verdon [11] have shown that it is possible to control the noise generated by wake/blade row interactions through the use of anti-sound actuators on the blade

surfaces from an analytical/numerical approach but no experimental results are available. Yu and Li [18] have also theoretically investigated the feasibility of reducing the gust/cascade interaction noise using dipolar secondary sources distributed on cascade surfaces. The amplitudes of the secondary sources are obtained from an aeroacoustic inverse model.

One can also note few studies discussing the active control of the free field radiation of small axial flow fans, like Lauchle et al. [12] who used a small baffled axial flow fan itself as a "crude loudspeaker". A near field microphone and a tachometer served as an error sensor and as a reference signal respectively. The acoustic pressure at the error microphone was reduced by 20 dB for the BPF, 15 dB for the first harmonic of the BPF and 8 dB for the second harmonic of the BPF. A directivity pattern shows that the fundamental tone radiation is attenuated in the whole half-space. Moreover, the sound power at the BPF and first harmonic was reduced by 13 and 8 dB, respectively. The main disadvantage of this technique for an automotive application is the use of a (bulky) shaker used to produce the anti-noise source and the potential coupling of vibrations with the environment of the fan such as the radiator. Quinlan [13], who modified the radiation impedance of the fan by placing a single secondary source close to the fan to reduce the acoustic energy propagating in the far field, globally attenuated the noise radiated by small axial flow fans. The A-weighted sound power level measured attenuations were 12 dB for the fundamental blade tone and 10 dB for the first BPF. The main constraint of this approach is the use of small fans since the distance between the two sources greatly affects the efficiency of the control system (the distance must be negligible compared to the acoustic wavelength to be controlled).

This paper addresses the issue of global control of engine cooling fan noise on the BPF and its first harmonic in free field. The approach use analytical and experimental investigations to demonstrate the feasibility of using a single loudspeaker in front of the fan to cancel the tonal noise. The engine cooling fans under investigation are six-bladed symmetric and seven-bladed non-symmetric fans with an external diameter given by $2a_2 = 30$ cm and a hub diameter given by $2a_1 = 12.5$ cm. Rotating speed of the fans is 50 Hz, so the blade passing frequency is 300 Hz and its first harmonic (2 BPF) is 600 Hz etc… for the six-bladed fan.

In this paper, a simplified analytical model is first used to describe the interference arising between the fan noise and the secondary source noise, and global control criteria in free field are defined. This model is however only valid when only the most radiating circumferential mode is considered. An important aspect of this research is the use of a direct-inverse aeroacoustic model presented in the companion paper [1] to calculate equivalent sources of a propeller for a non-homogeneous stationary flow field, which is the main phenomenon of tonal noise generation for subsonic fans. Using this model, active control simulations are conducted based upon the primary source extrapolated from the reconstructed unsteady forces given by the inverse aeroacoustic calculations to compare the radiated directivities with and without control (see also [16]). Finally, experimental results are presented to corroborate the simulations.

2. A simple active control model of free field fan noise

This section aims at simulating the acoustic interference resulting from a simplified, yet realistic description of the axial fan and a secondary (or control) source. Our starting point is a simplified,

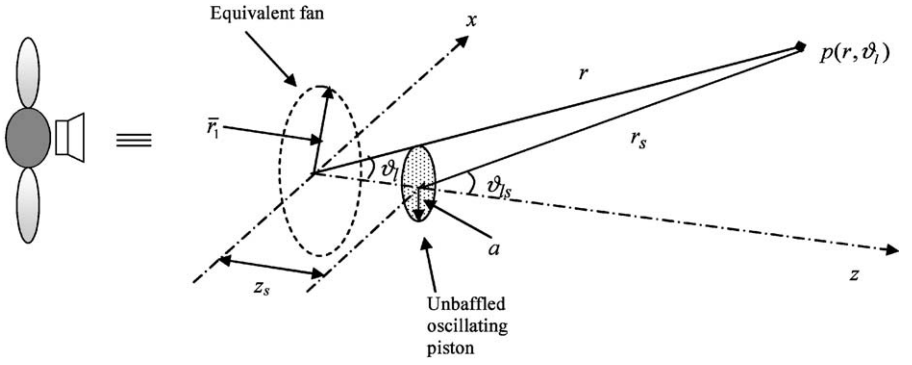

Fig. 1. Active control arrangement for free-field fan noise control.

axisymmetric free-field acoustic radiation pattern of the fan derived from the first part of this investigation [1], combined with a model of an unbaffled, co-axial oscillating piston as shown in Fig. 1. In what follows, the piston amplitude is calculated such that the sum of the resulting squared sound pressures $p(r,\vartheta_l)$ is minimised at L locations (r,ϑ_l) $(0\leqslant l\leqslant L)$ in the far field, where r and ϑ_l denote the distance from the fan centre and angle with respect to the fan axis, for the lth control point.

2.1. Simplified fan noise model

The far-field sound pressure at multiples of the fan blade passing frequency due to axial loading forces on the blades can be expressed from Eq. (6) of the companion paper [1]. However, several simplifications can lead to a more convenient form for preliminary analytical active control simulations. First, the fan effective area is reduced to an equivalent distribution of dipoles distributed along a mean radius of the fan $r_1=\bar{r}_1$. This approximation is expected to be accurate if the spatial extent of the fluctuating pressures is less than a wavelength of the sound generated and is probably also adequate for the spanwise distribution, unless there is a substantial change in phase across the fan span [17]. Also, only the zero-order Bessel function ($q=-nB$) is considered since it corresponds to the most radiating component in Eq. (6) of Ref. [1] for a subsonic fan. In this case, all the elementary radiating dipoles are in phase and the directivity of the radiation is a dipole normal to the plane of the propeller. Thus, the far-field acoustic pressure is symmetric with respect to the fan axis. Note that the index s of the companion paper has been replaced by n in this paper since s will serve as the secondary source subscript. It will be useful to consider the spectral components of the sound pressure at multiples n of the BPF. Considering the above simplifications, the primary sound field can be written $p_p(t;r,\vartheta)=\sum_n p_p(n\omega_1;r,\vartheta)\mathrm{e}^{-\mathrm{i}n\omega_1 t}$, with

$$p_p(n\omega_1;r,\vartheta)=-\mathrm{i}nk_1q_p\frac{\mathrm{e}^{\mathrm{i}nk_1r}}{4\pi r}J_0(nk_1\bar{r}_1\sin\vartheta)\cos\vartheta, \tag{1}$$

where $q_p=F_t\alpha_n(\bar{r}_1)\beta_{nB}(\bar{r}_1)$ is the primary complex source strength of the simplified primary source model and $F_t=\int_{a_1}^{a_2}f_z^0(r_1)2\pi r_1\mathrm{d}r_1$ is the total thrust of the propeller; $\omega_1=B\Omega$ is the BPF, B is the

number of blades, Ω is the fan rotational speed, $k_1 = \omega_1/c$, c is the sound speed. The n and q indices represent time and circumferential Fourier decompositions of the fluctuating forces in a fixed reference frame. The quantities α_n and β_q are the corresponding Fourier coefficients of the blade forces at a radial distance r_1 from the fan axis and f_z^0 is the time-averaged value of the blade force at a radial distance r_1. Moreover, a_1 and a_2 are the interior radius and exterior radius of the fan, respectively.

In the active control simulations, q_p is arbitrarily fixed to unity. Eq. (1) provides a simple analytical primary source model for tonal fan noise, which can be used to evaluate the performance of an active control system.

To anticipate the following development of a more realistic fan noise model (Section 5), Fig. 2 shows a comparison between the radiation field extrapolation derived from an inverse model of fan noise at BPF and at its first harmonic (1 and 2 BPF) [1] and the approximated radiation obtained by Eq. (1) (in-phase dipoles along a mean radial line). The directivities are compared to downstream measurement experimental data for the BPF and its first harmonic and show that under this particular loading condition (fan + radiator + rectangular obstruction behind the radiator), the simplified model is quite accurate for 1 BPF but is less precise for 2 BPF. However, under other fan loading conditions, the simplified model could be more accurate for 2 BPF. The rough approximation of Eq. (1) can serve as a first analysis of the active noise control without knowledge of experimental data, considering a dipolar sound radiation field for the first few harmonics of the BPF.

2.2. Secondary source model

If a single control source is assumed, it should be located close to the primary source and exhibit a similar spatial directivity. Since an axial fan operating at subsonic speeds roughly behaves like an equivalent dipole at first multiples of the BPF [1], another dipole radiating at the

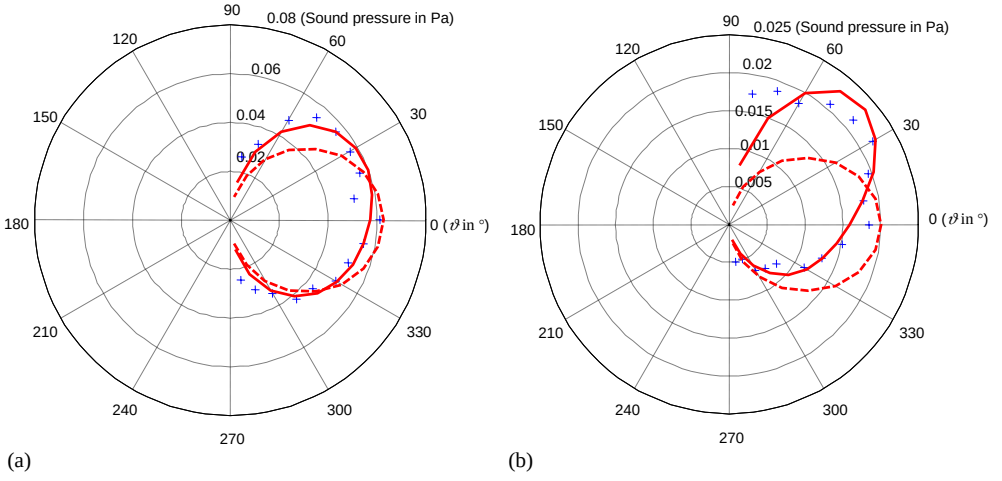

Fig. 2. Comparison between the simplified fan noise model of Eq. (1) (dashed line), the radiation field extrapolation from an inverse model of the fan (solid line) and experimental data (crosses). (a) BPF ($n = 1$), (b) 2 BPF ($n = 2$).

same set of frequencies but in opposite phase, close to the primary source is a good choice for globally controlling the sound field radiated by the fan. This can be achieved by using an unbaffled loudspeaker located at a distance z_s from the fan. A classical idealised model of an unbaffled loudspeaker is a circular piston of radius a radiating in free field as illustrated in Fig. 1. The far-field acoustic pressure of such a secondary source at a distance r_s from the piston centre and angle ϑ_s with respect to the piston axis is [14]

$$p_s(t; r_s, \vartheta_s) = \sum_n p_s(n\omega_1; r_s, \vartheta_s)\mathrm{e}^{-\mathrm{i}n\omega_1 t},$$

$$p_s(n\omega_1; r_s, \vartheta_s) = -\mathrm{i}nk_1 q_s \frac{\mathrm{e}^{\mathrm{i}nk_1 r_s}}{4\pi r_s}\left[\frac{2J_1(nk_1 a\sin\vartheta_s)}{nk_1 a\sin\vartheta_s}\right]\cos\vartheta_s, \tag{2}$$

where q_s is the amplitude of the force driving the piston, J_1 is the cylindrical Bessel function of order 1. For long wavelengths (relative to piston radius) the factor in brackets is approximately one. Thus the loudspeaker radiates like a point dipole oriented along the z-axis at low frequencies. Moreover, when $\vartheta_s = 0$, $ka\sin\vartheta_s = 0$ and the factor in brackets is also equal to 1.

2.3. Minimisation of the sum of squared pressures at far-field error microphone locations

In this section, the control source strength q_s is adjusted in order to minimise the total sound pressure at a number of far-field locations (r, ϑ_l) $(0 \leqslant l \leqslant L)$. Following Nelson [2], let us consider L error sensors in the far field and define the acoustic pressure vector

$$\mathbf{p} = [p(n\omega_1; r, \vartheta_l)\ldots p(n\omega_1; r, \vartheta_l)\ldots p(n\omega_1; r, \vartheta_L)]^{\mathrm{T}}, \tag{3}$$

where ϑ_l is the angular position of the lth sensor. The linear superposition principle is used to sum the contribution of the primary and the secondary fields in order to calculate the total sound pressure in the far field:

$$\mathbf{p} = \mathbf{z_p} q_p + \mathbf{z_s} q_s, \tag{4}$$

with $\mathbf{z_p}$ and $\mathbf{z_s}$ are the vectors of complex acoustic transfer function of the primary and the secondary sources respectively, defined by Eqs. (5) and (6)

$$\mathbf{z_p} = \left[-\mathrm{i}nk_1\frac{\mathrm{e}^{\mathrm{i}nk_1 r}}{4\pi r}J_0(nk_1\bar{r}_1\sin\vartheta_1)\cos\vartheta_1 \ldots - \mathrm{i}nk_1\frac{\mathrm{e}^{\mathrm{i}nk_1 r}}{4\pi r}J_0(nk_1\bar{r}_1\sin\vartheta_L)\cos\vartheta_L\right]^{\mathrm{T}}, \tag{5}$$

$$\mathbf{z_s} = \left[-\mathrm{i}nk_1\frac{\mathrm{e}^{\mathrm{i}nk_1 r_s}}{4\pi r_s}\left[\frac{2J_1(nk_1 a\sin\vartheta_{s1})}{nk_1 a\sin\vartheta_{s1}}\right]\cos\vartheta_{s1} \ldots - \mathrm{i}nk_1\frac{\mathrm{e}^{\mathrm{i}nk_1 r_s}}{4\pi r_s}\left[\frac{2J_1(nk_1 a\sin\vartheta_{sL})}{nk_1 a\sin\vartheta_{sL}}\right]\cos\vartheta_{sL}\right]^{\mathrm{T}}, \tag{6}$$

where r and r_s denote the distance of the lth sensor from the primary source and the secondary source, respectively. Moreover, ϑ_l and ϑ_{sl} denote the angle of the lth sensor with respect to the z-axis from the primary and secondary source, respectively. We introduce a cost function equal to the sum of the squared acoustic pressures at the L sensors, for each integer

multiple n of the BPF ω_1:

$$J_p = \sum_{l=1}^{L} |p(n\omega_1; r, \vartheta_l)|^2 = \mathbf{p}^{\mathbf{H}}\mathbf{p}, \tag{7}$$

in which the superscript H is the Hermitian operator.

Substituting Eq. (4) into Eq. (7) leads to a quadratic Hermitian function of the complex secondary source strength [2]:

$$J_p = |q_p|^2 \mathbf{z}_{\mathbf{p}}^{\mathbf{H}}\mathbf{z}_{\mathbf{p}} + q_p^* \mathbf{z}_{\mathbf{p}}^{\mathbf{H}}\mathbf{z}_{\mathbf{s}} q_s + q_s^* \mathbf{z}_{\mathbf{s}}^{\mathbf{H}}\mathbf{z}_{\mathbf{p}} q_p + |q_s|^2 \mathbf{z}_{\mathbf{s}}^{\mathbf{H}}\mathbf{z}_{\mathbf{s}}, \tag{8}$$

where * is the complex conjugate symbol. Since $\mathbf{z}_{\mathbf{s}}^{\mathbf{H}}\mathbf{z}_{\mathbf{s}}$ is a positive quantity, J_p has a unique global minimum which is obtained for an optimal control force driving the piston, equal to

$$q_{s0} = -\frac{\mathbf{z}_{\mathbf{s}}^{\mathbf{H}}\mathbf{z}_{\mathbf{p}}}{\mathbf{z}_{\mathbf{s}}^{\mathbf{H}}\mathbf{z}_{\mathbf{s}}}\, q_p. \tag{9}$$

The optimal control source strength can be somewhat simplified by using the following far field approximations in Eqs. (5) and (6): $\vartheta_{sl} \approx \vartheta_l$, $r_s \approx r$ in the denominator of Eqs. (5) and (6), and $r_s \approx r - z_s \cos\vartheta_l$ in the exponential term of Eqs. (5) and (6). After some algebra, Eq. (9) leads to

$$q_{s0} = -q_p \frac{\sum_{l=1}^{L} \mathrm{e}^{\mathrm{i}nk_1 z_s \cos\vartheta_l} J_0(nk_1 \bar{r}_1 \sin\vartheta_l) \left(\frac{2J_1(nk_1 a \sin\vartheta_l)}{nk_1 a \sin\vartheta_l}\right) \cos^2\vartheta_l}{\sum_{l=1}^{L} \left(\frac{2J_1(nk_1 a \sin\vartheta_l)}{nk_1 a \sin\vartheta_l}\right)^2 \cos^2\vartheta_l}. \tag{10}$$

2.4. Case $L = 1$

If $L = 1$ (one error microphone located at (r, ϑ_0)), Eq. (10) reduces to

$$q_{s0} = -q_P \left[\frac{nk_1 a \sin\vartheta_0}{2J_1(nk_1 a \sin\vartheta_0)}\right] J_0(nk_1 \bar{r}_1 \sin\vartheta_0) \mathrm{e}^{\mathrm{i}nk_1 z_s \cos\vartheta_0} \tag{11}$$

If $\vartheta_0 = 0$, the term in bracket is unity. Thus, the resulting sound pressure field when Eq. (11) is satisfied is given by

$$p(n\omega_1; r, \vartheta) = \begin{cases} p_p(n\omega_1; r, \vartheta)\left(1 - \frac{J_0(nk_1 \bar{r}_1 \sin\vartheta_0)}{J_1(nk_1 a \sin\vartheta_0)} \frac{J_1(nk_1 a \sin\vartheta)}{J_0(nk_1 \bar{r}_1 \sin\vartheta)} \frac{\sin\vartheta_0}{\sin\vartheta} \mathrm{e}^{\mathrm{i}nk_1 z_s(\cos\vartheta_0 - \cos\vartheta)}\right), \\ \quad \vartheta_0 \neq 0, \vartheta \neq 0, \\ p_p(n\omega_1; r, \vartheta)\left(1 - \frac{1}{J_0(nk_1 \bar{r}_1 \sin\vartheta)} \frac{2J_1(nk_1 a \sin\vartheta)}{nk_1 a \sin\vartheta} \mathrm{e}^{\mathrm{i}nk_1 z_s(1 - \cos\vartheta)}\right), \\ \quad \vartheta_0 = 0, \vartheta \neq 0, \\ p_p(n\omega_1; r, \vartheta)\left(1 - J_0(nk_1 \bar{r}_1 \sin\vartheta_0) \frac{nk_1 a \sin\vartheta_0}{2J_1(nk_1 a \sin\vartheta_0)} \mathrm{e}^{\mathrm{i}nk_1 z_s(\cos\vartheta_0 - 1)}\right), \\ \quad \vartheta_0 \neq 0, \vartheta = 0, \\ 0, \quad \vartheta_0 = 0, \vartheta = 0, \end{cases} \tag{12}$$

where p_p denotes the primary sound field given by Eq. (1). Eq. (12) gives a general expression of the resulting field as a function of the primary and secondary source arrangement. It provides a useful analytical formulation for preliminary investigations of active control of fan noise using an unbaffled loudspeaker.

For long wavelength approximation ($\lambda \gg a, \bar{r}_1$) Eq. (12) can be reduced to a simpler form:

$$p(n\omega_1; r, \vartheta) \approx p_p(n\omega_1; r, \vartheta)(1 - e^{ink_1 z_s(\cos\vartheta_0 - \cos\vartheta)}), \tag{13}$$

with $p_p(n\omega_1; r, \vartheta) \approx -ink_1 q_p(e^{ink_1 r}/4\pi r)\cos\vartheta$. At low frequency, both the fan and the control loudspeaker radiate like point dipoles. From Eq. (13), the condition for global attenuation of the resulting sound field in the entire far field is the same as for two monopole sources: $k_1 z_s < \pi/6$ or $12 < \lambda/z_s$ [2].

3. Far-field sound directivity after control

Numerical results of active control simulation are presented in this section. The configuration investigated corresponds to the sound radiation of a typical automotive engine cooling axial fan ($\bar{r}_1 = 12$ cm) in the frequency range 0–700 Hz that includes 1 and 2 BPF. A control piston of radius $a = 4$ cm is located at a distance $z_s = 5$ cm from the fan. This arrangement corresponds to the experimental set-up presented in Section 6 of this paper. For this configuration, $10 < \lambda/z_s$, $12 < \lambda/a$ and $4 < \lambda/\bar{r}_1$, therefore the above theoretical conditions for global control are reasonably well satisfied. In the simulations, the primary source strength is fixed to $q_p = 1$, and the secondary source strength is calculated from Eq. (10) or Eq. (11). The results are plotted in terms of the far-field sound directivity with and without control.

3.1. Case $L = 1$

Fig. 3 shows the directivity plots in the case of $L = 1$ single far-field error microphone at various angular positions $\vartheta_0 = 0, \pi/6, \pi/3$ in the downstream half-space. The left column is obtained for a frequency $f = 300$ Hz and the right column for $f = 600$ Hz; these values correspond respectively to $n = 1$ and 2 in the case of a six-bladed axial fan operating at a rotating speed of 50 Hz. In the case of the left column, $\lambda/z_s \approx 23$, $\lambda/a \approx 28$ and $\lambda/\bar{r}_1 \approx 9.4$, and both the primary and control sources almost behave as point dipoles in this case. The spatial directivity of the control source in Fig. 3 reasonably matches the directivity of the fan, resulting in a significant sound attenuation in the error microphone half-space. The best global attenuation in the downstream half-space is obtained for $\vartheta_0 = \pi/6$ in this case. The downstream directivity in the case $\vartheta_0 = 0$ is typical of a weakly radiating equivalent quadrupole source. Note however that the control performance is generally much less in the upstream half-space.

In the case of the right column of Fig. 3 ($f = 600$ Hz), $\lambda/z_s \approx 11$, $\lambda/a \approx 14$ and $\lambda/\bar{r}_1 \approx 4.7$. The spatial extent of the primary source and secondary source become important and their radiation is not perfectly dipolar. The control performance is significantly less than for $f = 300$ Hz but appreciable global reduction of the downstream sound field can still be achieved especially for $\vartheta_0 = 0$ and $\vartheta_0 = \pi/6$. Moderate or negligible reduction is observed in the upstream half-space.

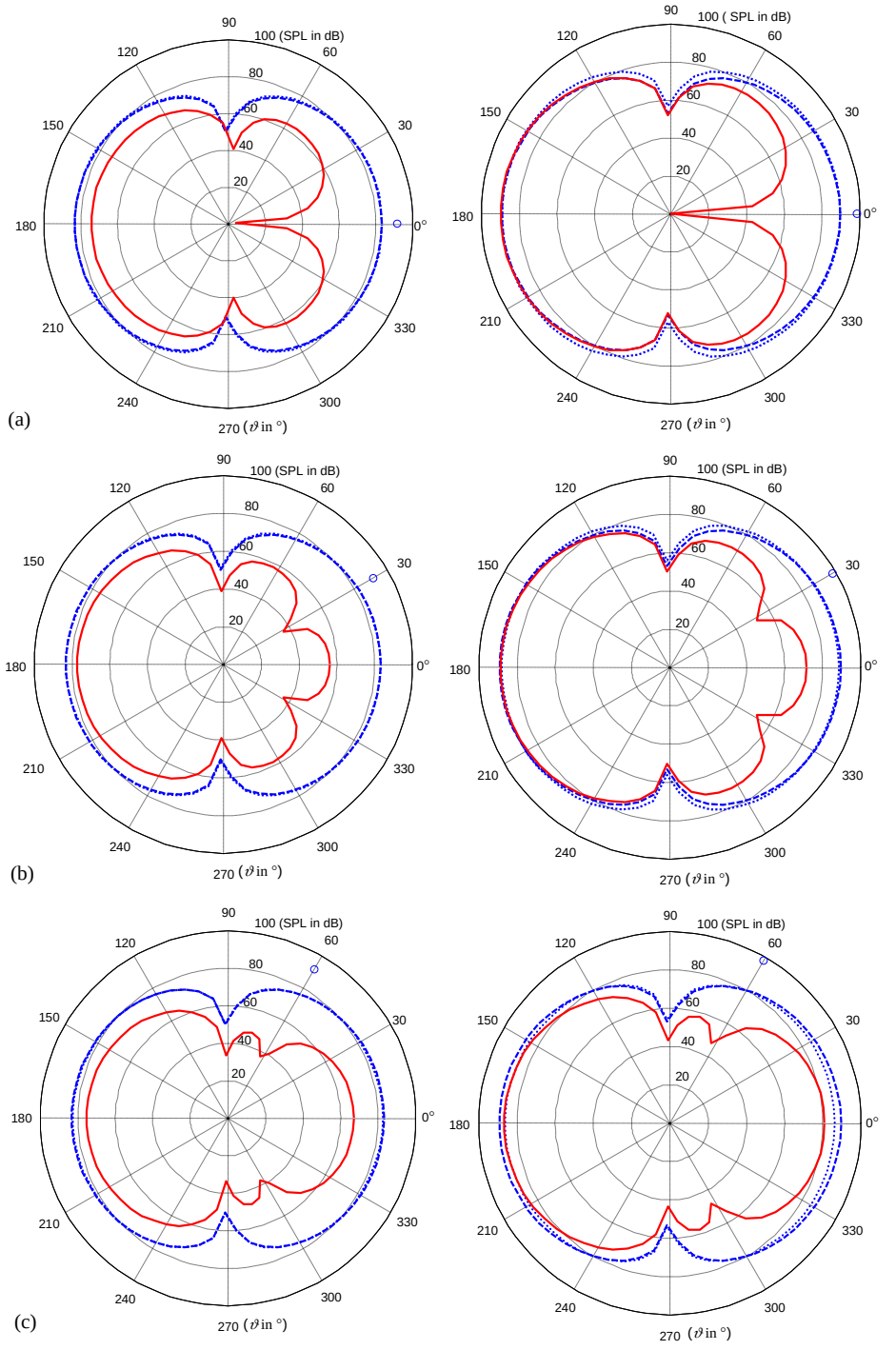

Fig. 3. Far-field sound directivity in the case $L = 1$ for various error sensor positions. Primary source (dashed line), secondary source (dotted line) and global (solid line). Left-hand column: $f = 300\,\text{Hz}$, $\lambda/z_s \approx 23$, $\lambda/a \approx 28$ and $\lambda/\bar{r}_1 \approx 9.4$. Right-hand column: $f = 600\,\text{Hz}$; $\lambda/z_s \approx 11$, $\lambda/a \approx 14$ and $\lambda/\bar{r}_1 \approx 4.7$. (a) $\theta_0 = 0$; (b) $\theta_0 = \pi/6$; (c) $\theta_0 = \pi/3$.

In summary, a single secondary unbaffled oscillating piston is able to match the radiation pattern of a simple model of a typical engine cooling fan in the frequency range 0–600 Hz. Therefore, it is expected that a single control source and a single far-field error microphone are effective in controlling the downstream sound field of such a fan.

3.2. Case $L>1$

In order to more effectively control both the upstream and downstream sound fields, it may be appropriate to introduce a number of far-field error microphones distributed in several directions ϑ_l $(0 \leqslant l \leqslant L)$. Fig. 4 shows the directivity plots for the same primary and secondary source

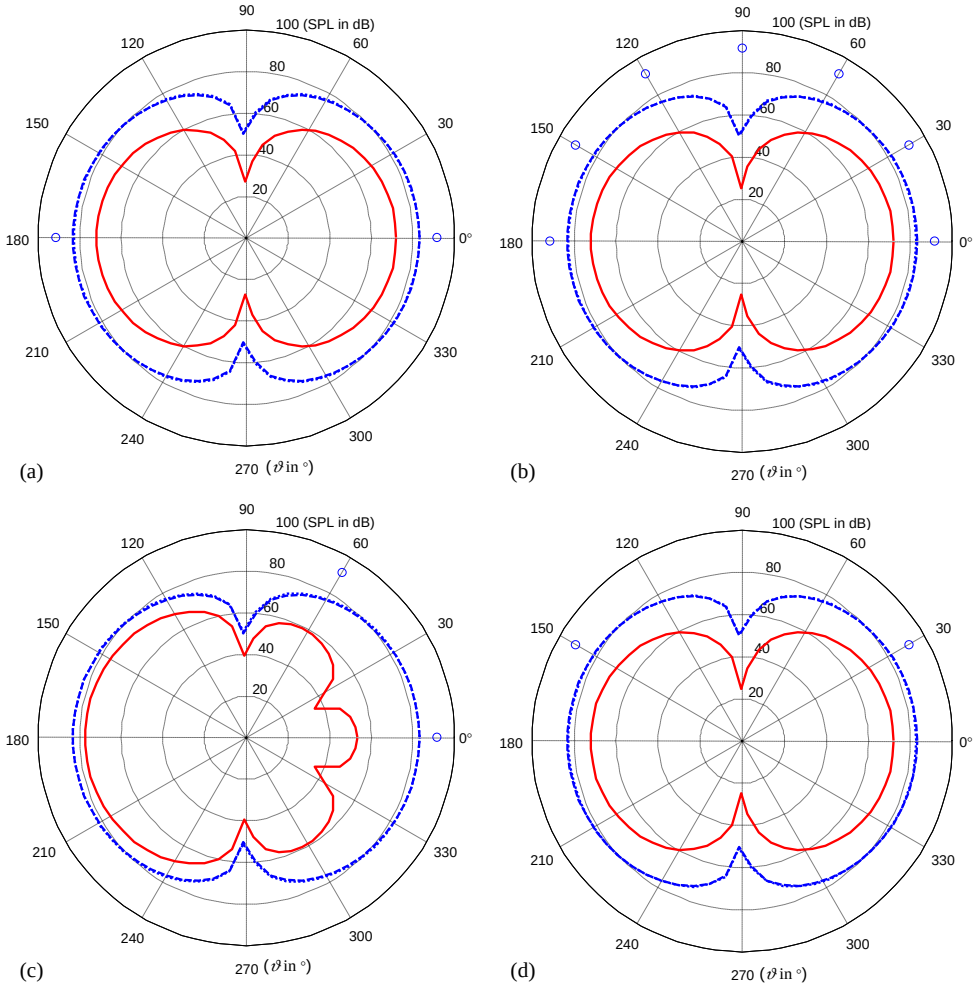

Fig. 4. Far-field sound directivity at $f = 300$ Hz in the case $L>1$ for various error sensor positions: (a) $\vartheta_1 = 0$ and $\vartheta_2 = \pi$, (b) $\vartheta_l = l\pi/6$, $l = [0, 1, 2, 3, 4, 5, 6]$, (c) $\vartheta_1 = 0$ and $\vartheta_2 = \pi/3$, (d) $\vartheta_1 = \pi/3$ and $\vartheta_2 = 5\pi/6$. Primary source (dashed line), secondary source (dotted line, quasi-superimposed to the primary directivity) and global (solid line); $\lambda/z_s \approx 11$, $\lambda/a \approx 14$ and $\lambda/\bar{r}_1 \approx 4.7$.

arrangement as previously, but with several error microphones distributed in the upstream or downstream half-space. The secondary source in this case is adjusted to minimise the sum of the squared pressures at the error sensors. The disturbance frequency in Fig. 4 is $f = 300\,\text{Hz}$, therefore $\lambda/z_s \approx 23$, $\lambda/a \approx 28$ and $\lambda/\bar{r}_1 \approx 9.4$ as in left column of Fig. 3. These results indicate that several error sensors distributed in the whole space are effective in controlling both the upstream and downstream sound radiation (the primary and secondary directivities are nearly coincident). However, when comparing the results of Figs. 3 and 4, one notes that if the objective is to reduce the radiation in the downstream half-space only, then adding more error sensors in this half-space does not significantly improve the control performance. This observation is however closely related to the axial symmetry of the simplified aeroacoustic model of the fan. In reality, a non-uniform upstream flow entering the fan translates into a non-axially symmetric directivity of the primary sound field [1]. Therefore, the control effectiveness when using an axially symmetric control source may be decreased in this case. However, this simple model provides a useful tool for a preliminary design and understanding of the tonal fan noise active control when a loudspeaker is located in front of the fan.

4. Metrics for global control

4.1. Far-field sound pressure

Following Nelson [2] for the case of two coupled monopoles, it is possible to compare the squared far-field sound pressure produced by the interference of the two sources $|p(r,\vartheta)|^2$ to that produced by the fan alone $|p_p(r,\vartheta)|^2$ for any direction ϑ, from Eq. (12) for $L = 1$ or from Eq. (4) for $L > 1$. The condition for a global attenuation of the sound field in all directions is given by

$$\eta = \frac{|p(r,\vartheta)|^2}{|p_p(r,\vartheta)|^2} < 1 \quad \forall\vartheta. \tag{14}$$

In order to illustrate the effectiveness of the active control in the far field, the parameter $\log\eta$ is plotted in Fig. 5 as a function of the direction $-\pi \leqslant \vartheta \leqslant \pi$ and the non-dimensional wavelength λ/z_s in the case of $L = 1$ error sensor for two different locations of the error sensor: $\vartheta_0 = 0$ and $\vartheta_0 = \pi/4$. The configuration investigated is similar to the previous section, and representative of an actual engine cooling fan (mean radius of the fan $\bar{r}_1 = 12\,\text{cm}$, control piston of radius $a = 4\,\text{cm}$ at $z_s = 5\,\text{cm}$ from the fan centre). The horizontal plane $\log\eta = 0$ is also plotted in Fig. 5 in order to illustrate the limit for global control: configurations for which $\log\eta < 0$ correspond to a sound pressure attenuation and $\log\eta > 0$ are associated to a sound pressure increase in the corresponding direction. In the case $\vartheta_0 = 0$, a sound pressure attenuation is obtained in all directions as long as $\lambda/z_s > 13$; when $\lambda/z_s \leqslant 13$, an increased sound pressure is observed in the directions near $\vartheta = \pm\pi/2$, i.e. near the plane of the fan. In the case $\vartheta_0 = \pi/4$, the condition for global sound pressure attenuation is slightly less stringent, $\lambda/z_s > 11$; for smaller wavelength, a sound pressure reinforcement is also observed near $\vartheta = \pm\pi/2$. For a source separation $z_s = 5\,\text{cm}$, the condition $\lambda/z_s > 13$ ($\vartheta_0 = 0$) implies an upper frequency limit of about 520 Hz for global sound pressure attenuation, whereas $\lambda/z_s > 11$ ($\vartheta_0 = \pi/4$) implies an upper limit of about 620 Hz. These values

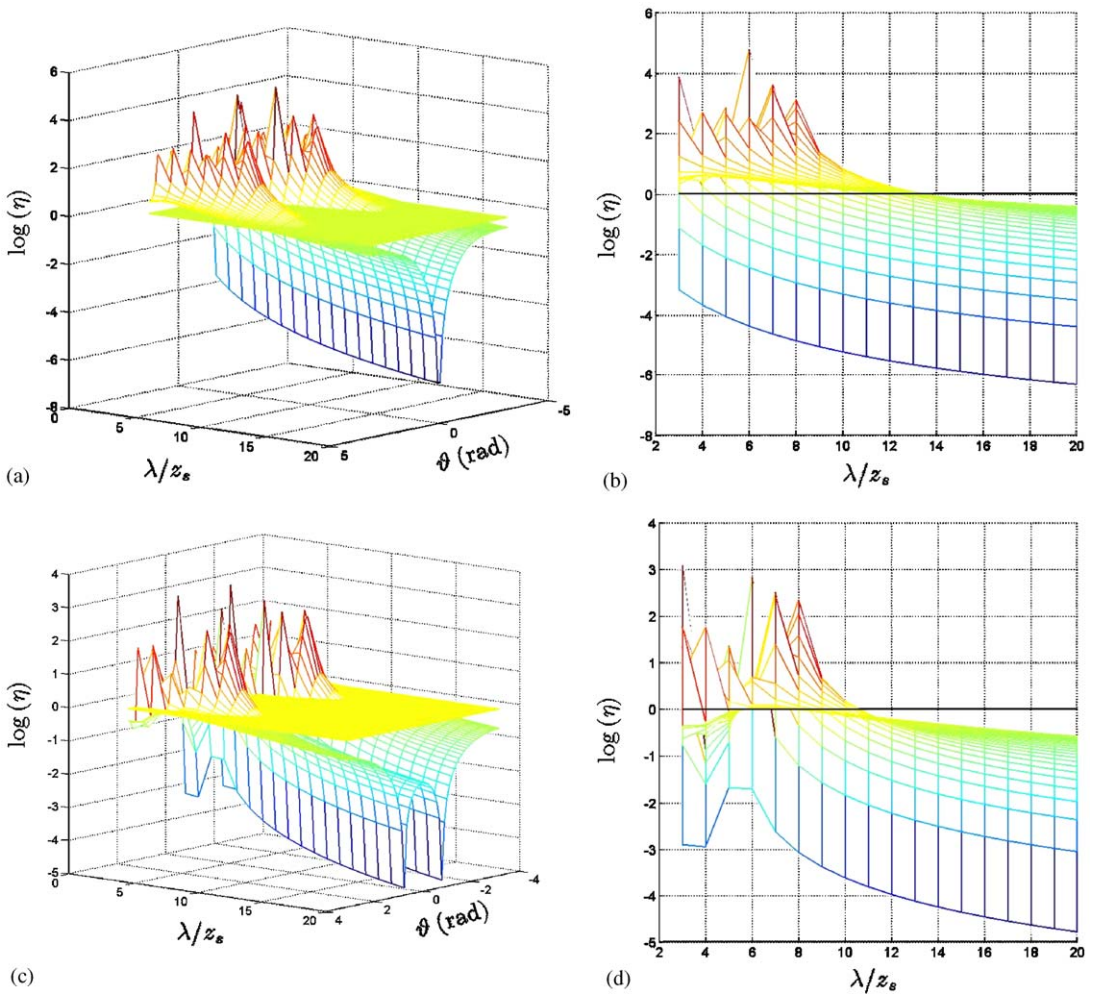

Fig. 5. Control parameter $\log(\eta)$ as a function of far-field direction ϑ and non-dimensional wavelength λ/z_s for $L = 1$, $\bar{r}_1 = 12$ cm, $a = 4$ cm, $z_s = 5$ cm. (a) 3-D view point, $\vartheta_0 = 0$, (b) projection in the plane $(\log(\eta), \lambda/z_s)$, $\vartheta_0 = 0$, (c) 3-D view point, $\vartheta_0 = \pi/4$, (d) projection in the plane $(\log(\eta), \lambda/z_s)$, $\vartheta_0 = \pi/4$.

suggest that such a SISO active control arrangement is able to globally reduce the first 2 tones of a six-bladed automotive fan operating at a rotational speed of 50 Hz in free field.

4.2. Sound power

Another quantity of interest to evaluate the global control performance is the sound power attenuation. A reduction by the active control system of the total sound power is a less constraining condition than a reduction of the far-field sound pressure in all directions. The total sound power of the primary and secondary source combination is related to the far-field sound

pressure $p(r,\vartheta)$ by

$$W = \frac{1}{2}\int_0^{\pi}\int_0^{2\pi} \frac{|p(r,\vartheta)|^2}{\rho c}\, r^2 \sin\vartheta \,\mathrm{d}\vartheta \,\mathrm{d}\varphi, \tag{15}$$

where ρ is the mass density of air and φ is a spherical coordinate defined in Fig. 1 of Ref. [1]. The r dependence disappears in W because the far-field sound pressure $p(r,\vartheta)$ is inversely proportional to r. Moreover the simplified primary and control source models imply that the radiated sound field is axially symmetric, thus

$$W = \frac{\pi r^2}{\rho c}\int_0^{\pi} |p(r,\vartheta)|^2 \sin\vartheta \,\mathrm{d}\vartheta. \tag{16}$$

The integral in Eq. (16) needs to be evaluated numerically from the far-field sound pressure obtained from Eq. (12) for $L = 1$ or from Eq. (4) for $L > 1$, using I discrete values of ϑ_i spaced by $\Delta\vartheta$, $W = (\pi r^2/\rho c)\Delta\vartheta\sum_{i=1}^{I}|p(r,\vartheta_i)|^2 \sin\vartheta_i$. We then define a new control parameter η_W as the ratio of the sound power with and without control,

$$\eta_W = \frac{W}{W_p}. \tag{17}$$

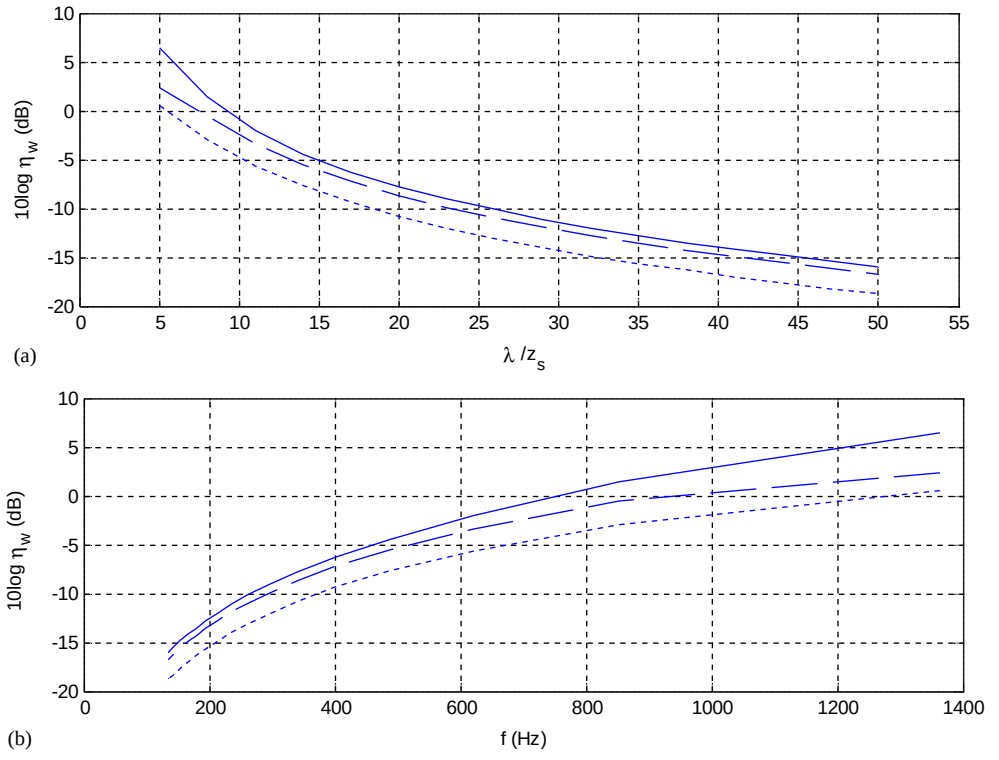

Fig. 6. (a) Sound power parameter $10\log\eta_W$ as a function of non-dimensional wavelength λ/z_s and (b) $10\log\eta_W$ as a function of frequency for $L = 1$, $\bar{r}_1 = 12$ cm, $a = 4$ cm, $z_s = 5$ cm and for various error microphone directions $\vartheta_0 = 0$ (solid line), $\vartheta_0 = \pi/6$ (dashed line), $\vartheta_0 = \pi/3$ (dotted line).

Fig. 6 shows the value of $10\log\eta_W$ as a function of the non-dimensional wavelength λ/z_s (top graph) or frequency (bottom graph) for the same problem as before (mean radius of the fan $\bar{r}_1 = 12$ cm, control piston of radius $a = 4$ cm at $z_s = 5$ cm from the fan centre), and for $L = 1$ far-field error microphone located at various directions $\vartheta_0 = 0, \pi/6, \pi/3$. It is seen that more oblique directions of the error sensor with respect to the fan axis yield better sound power attenuation after control. Also, a reduction of the sound power is obtained when $\lambda/z_s > 9$ for $\vartheta_0 = 0$, when $\lambda/z_s > 8$ for $\vartheta_0 = \pi/6$ and when $\lambda/z_s > 5.5$ for $\vartheta_0 = \pi/3$ (corresponding to $f = 750$ Hz, $f = 970$ Hz and $f = 1270$ Hz, respectively in the particular arrangement of the present study). These conditions are slightly less restrictive than imposing a reduction of the far-field sound pressure in *all* directions of space, as discussed in Section 4.1. For such a six-bladed automotive fan operating at a rotational speed of 50 Hz, a one control loudspeaker—one error microphone system would optimally provide a sound power difference ($10\log\eta_W$) between -9 and -13 dB at 1 BPF (300 Hz), and between -2 and -6 dB at 2 BPF (600 Hz).

Fig. 7 shows similar results when more error sensors are added ($L = 2$). These results show that two cancellation points symmetrically located upstream and downstream on the fan axis ($\vartheta_1 = 0$ and $\vartheta_2 = \pi$) give the best attenuation of the total sound power. In this configuration, the active control would provide a sound power difference ($10\log\eta_W$) of -13dB at 300 Hz, and -7 dB at 600 Hz. The additional gain with respect to a single downstream error microphone is thus marginal.

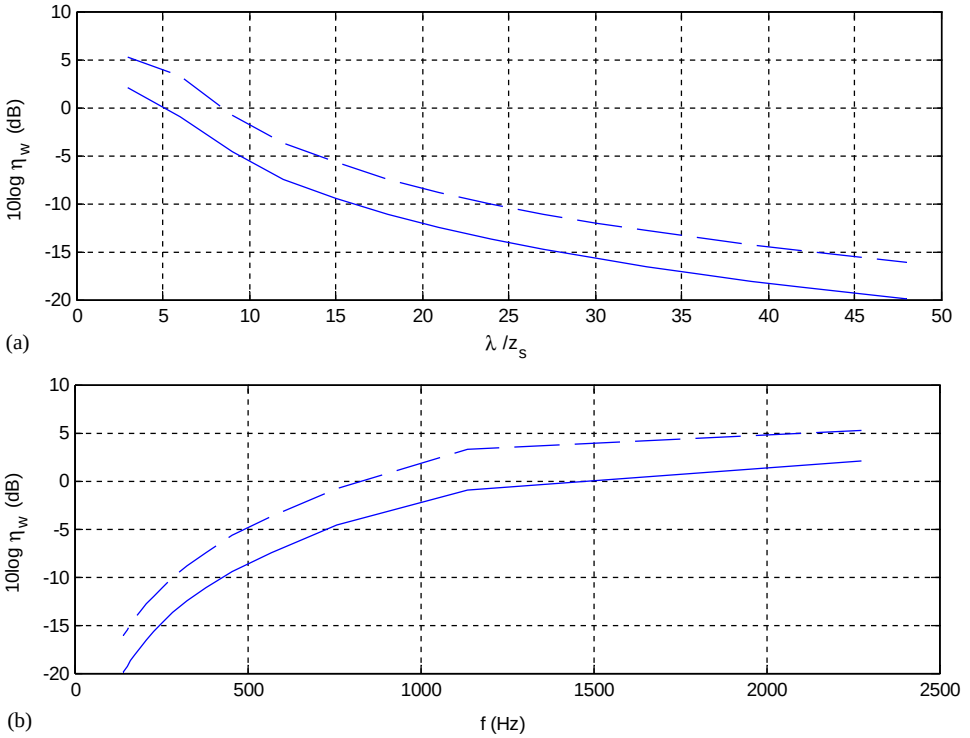

Fig. 7. (a) Sound power parameter $10\log\eta_W$ as a function of non-dimensional wavelength λ/z_s and (b) $10\log\eta_W$ as a function of frequency for $\bar{r}_1 = 12$ cm, $a = 4$ cm, $z_s = 5$ cm and for various error microphone arrangements: $L = 2$, $\vartheta_1 = 0$ and $\vartheta_2 = \pi$ (solid line); $L = 2$, $\vartheta_1 = 0$ and $\vartheta_2 = \pi/3$ (dashed line).

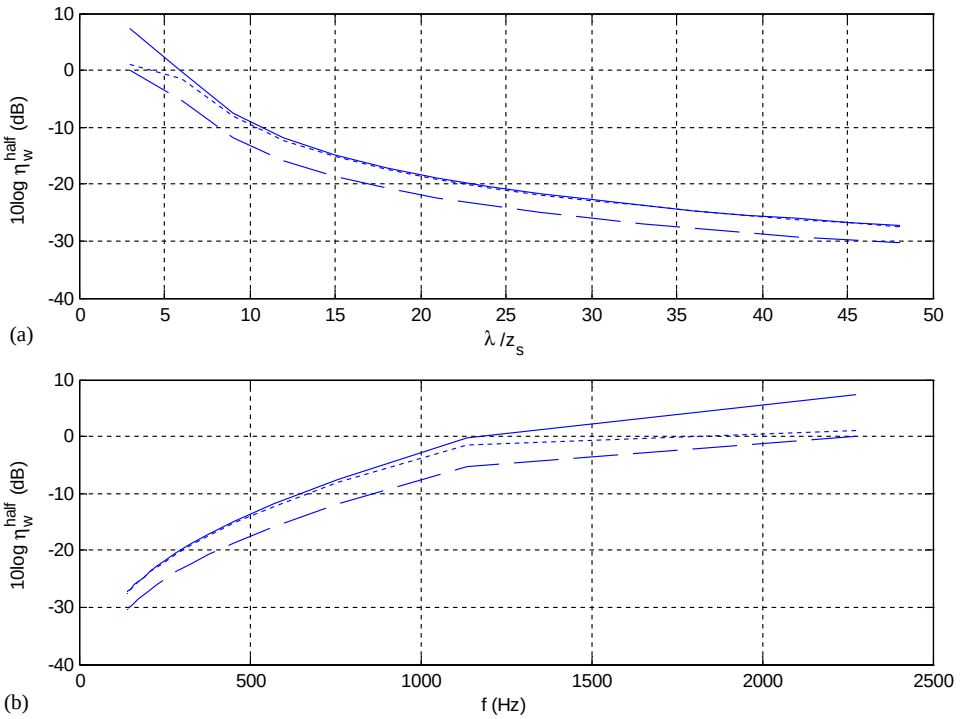

Fig. 8. (a) Half-space sound power parameter $10\log\eta_W^{\text{half}}$ as a function of non-dimensional wavelength λ/z_s and (b) $10\log\eta_W^{\text{half}}$ as a function frequency for $L=1$, $\bar{r}_1=12\,\text{cm}$, $a=4\,\text{cm}$, $z_s=5\,\text{cm}$ and for various error microphone directions $\vartheta_0=0$ (solid line); $\vartheta_0=\pi/6$ (dashed line); $\vartheta_0=\pi/3$ (dotted line).

Certain practical situations require that the sound field be controlled in just a half-space (e.g. downstream). In this case, it is more appropriate to introduce a modified half-space sound power parameter $\eta_W^{\text{half}}=W^{\text{half}}/W_p^{\text{half}}$ in which W^{half} and W_p^{half} are the sound power radiated in a half-space with and without control and are obtained by carrying the integration over $0\leqslant\vartheta\leqslant\pi/2$ in Eq. (16). Fig. 8 shows the corresponding half-space control performance $10\log\eta_W^{\text{half}}$ when only $L=1$ downstream error sensor is used in various directions $\vartheta_0=0$, $\pi/6$, $\pi/3$. It is clear that an increased control performance can be obtained by relaxing the constraint of upstream sound field reduction. In this case, a single downstream error microphone is able to provide a downstream sound power reduction when $\lambda/z_s>6$ for $\vartheta_0=0$, $\lambda/z_s>3$ for $\vartheta_0=\pi/6$, $\lambda/z_s>4.5$ for $\vartheta_0=\pi/3$. The optimal downstream sound power reduction is between -20 and $-23\,\text{dB}$ at 300 Hz and between -11 and $-16\,\text{dB}$ at 600 Hz.

5. Active control simulations using the inverse aeroacoustic model

The previous simulations are based on a simple fan noise model which only takes into account the circumferential mode $q=-nB$ in the calculation of the radiated sound field, Eq. (1). This assumption implies that the acoustic directivity is axially symmetric and has a maximum on the

fan axis. Therefore it is expected that a secondary dipole source located in front of the fan is able to match this primary directivity pattern and is sufficient to provide an effective sound attenuation. In reality, other circumferential modes ($q \neq -nB$) may contribute significantly to sound radiation for non-homogeneous flow. This results in a non-axially symmetric radiation directivity that can be more accurately predicted making use of the inverse model [1]. In this section, the inverse model is used to obtain a continuous extrapolated sound field from a discrete set of measurement points through the reconstruction of the forces acting by the blades on the fluid [1]. The continuous primary sound field is then combined with the secondary sound field to derive the resulting field and to simulate optimal active control of fan tones.

We start with the general expression of the primary multi-tonal fan noise in spherical coordinates (r, φ, ϑ), $p_p(t; r, \varphi, \vartheta) = \sum_n p_p(n\omega_1; r, \varphi, \vartheta)\mathrm{e}^{-\mathrm{i}n\omega_1 t}$, where $\omega_1 = B\Omega$ is the blade passing frequency and according to Eq. (6) of the companion paper [1],

$$p_p(n\omega_1; r, \varphi, \vartheta) = -\frac{\mathrm{i}k_1 \cos\vartheta}{4\pi r} \sum_{q=-\infty}^{+\infty} \mathrm{i}^{nB+q} \mathrm{e}^{\mathrm{i}nk_1 r} \mathrm{e}^{\mathrm{i}(nB+q)\varphi} \times \int_{a_1}^{a_2} nf_z^0(r_1)\alpha_n(r_1)\beta_q(r_1) J_{nB+q}(nk_1 r_1 \sin\vartheta) 2\pi r_1 \, \mathrm{d}r_1. \tag{18}$$

Following Ref. [1], it is possible to write

$$p_p(n\omega_1; r, \varphi, \vartheta) = -\mathrm{i}nk_1 q_p \frac{\mathrm{e}^{\mathrm{i}nk_1 r}}{4\pi r} \cos\vartheta, \tag{19}$$

where

$$q_p = -\sum_{q=-\infty}^{+\infty} \sum_i \mathrm{i}^{nB+q} \mathrm{e}^{\mathrm{i}(nB+q)\varphi} f_z^0(r_{1i})\alpha_n(r_{1i})\beta_q(r_{1i}) J_{nB+q}(nk_1 r_{1i} \sin\vartheta) 2\pi r_{1i} \Delta r_1$$

is the complex primary source at the nth multiple of the BPF, i denotes discretization of the radial coordinate over the fan area and r_{1i} are I equally spaced points in the interval $[a_1 a_2]$ with a step of Δr_1. The value of the source terms $f_z^0(r_{1i})\alpha_n(r_{1i})\beta_q(r_{1i})$ in q_p is adjusted to fit measured far-field sound pressure data as discussed in Ref. [1].

The same secondary source model as before is assumed (unbaffled oscillating piston), therefore,

$$p_s(n\omega_1; r, \vartheta) = -\mathrm{i}nk_1 q_s \frac{\mathrm{e}^{\mathrm{i}nk_1 r_s}}{4\pi r_s} \left[\frac{2J_1(k_1 a \sin\vartheta)}{k_1 a \sin\vartheta}\right] \cos\vartheta,$$

where q_s is the strength of the control source. Combining the primary and secondary sound field,

$$p(n\omega_1; r, \varphi, \vartheta) = p_p(n\omega_1; r, \varphi, \vartheta) + p_s(n\omega_1; r, \vartheta) = -\mathrm{i}nk_1 \frac{\mathrm{e}^{\mathrm{i}nk_1 r}}{4\pi r} \cos\vartheta \left(q_p + q_s \mathrm{e}^{-z_s \cos\vartheta} \left[\frac{2J_1(k_1 a \sin\vartheta)}{k_1 a \sin\vartheta}\right] \right). \tag{20}$$

The secondary source strength is adjusted to minimise the far-field squared sound pressure at a number of far-field locations (r, ϑ_l) $(0 \leqslant l \leqslant L)$, as discussed in Section 2.3. The expression

of $\mathbf{z_p}$ becomes

$$\mathbf{z_p} = \left[-\mathrm{i}nk_1 \frac{\mathrm{e}^{\mathrm{i}nk_1 r}}{4\pi r} \cos\vartheta_1 \cdots - \mathrm{i}nk_1 \frac{\mathrm{e}^{\mathrm{i}nk_1 r}}{4\pi r} \cos\vartheta_L \right]^{\mathrm{T}}. \tag{21}$$

5.1. Six-bladed fan with equal blade pitches

The simulation presented here involves primary source data which have been derived from directivity measurements of a six-bladed fan ($B = 6$) with equal blade pitches. The actual fan has a radius $R = 15\,\mathrm{cm}$ and a 12.5 cm diameter central hub. The rotational speed has been fixed to $\Omega = 50\,\mathrm{Hz}$ so that the first 2 disturbing tones are at 1 BPF = 300 Hz and 2 BPF = 600 Hz. In order to identify the inverse aeroacoustic model of the fan, the acoustic directivity of the fan was measured in an anechoic room at 17 regularly spaced points on a circular arc at 1.5 m from the fan centre, with $\varphi = 0$ and $-80^\circ < \vartheta < 80^\circ$ in the downstream half-space. Fig. 9 shows directivity plots for the fan alone (as derived from the inverse aeroacoustic model), the adjusted secondary source and the two optimally combined sources. The control loudspeaker arrangement is similar to the previous sections ($a = 4\,\mathrm{cm}$ and $z_s = 5\,\mathrm{cm}$) and $L = 1$ error microphone was considered at $\vartheta_0 = 0$, $\pi/4$ in the downstream half-space. The directivity plots show that the primary sound field is not axially symmetric, whereas the secondary source directivity remains symmetric. Consequently, the control performance is degraded as compared to the simplified primary source model of Figs. 2 and 3. However, trends are similar and the control is still global in the downstream half-space with only one cancellation point and one secondary source. For the BPF, the simulated sound power reductions are about -10.8 and $-13.8\,\mathrm{dB}$ when the error microphone are located at $\vartheta = 0$ and $\vartheta = \pi/4$, respectively. As far as 2 BPF is concerned, the reductions are -4.8 and $-5.8\,\mathrm{dB}$ for $\vartheta = 0$ and $\vartheta = \pi/4$, respectively. The choice of the error sensor location can therefore be optimised for a frequency while deteriorating the control of the other frequency to be controlled. The simulated attenuations from the inverse model are less than the modified half-space sound power parameter $10\log\eta_W^{\mathrm{half}}$ calculated from the simplified fan noise model in that case.

5.2. Seven-bladed fan with unequal blade pitches

The results presented in this section involve a seven-bladed fan ($B = 7$) with unequal blade pitches. Unequal blade pitches ensure a lower tonal sound radiation at integer multiples of the blade passing frequency but on the other hand generate additional tones at multiples of the rotational speed. The fan has a radius $R = 15\,\mathrm{cm}$ and a 12.5 cm diameter central hub. The rotational speed has been fixed to $\Omega = 48.5\,\mathrm{Hz}$ so that 2 most important disturbing tones are at 1 BPF = 340 Hz and 2 BPF = 680 Hz. The same experimental procedure as for the six-bladed fan was used to identify the inverse aeroacoustic model. Fig. 10 shows directivity plots for the fan alone (as derived from the inverse aeroacoustic model), the adjusted secondary source and the two optimally combined sources. The control loudspeaker arrangement is similar to previously ($a = 4\,\mathrm{cm}$ and $z_s = 5\,\mathrm{cm}$) and $L = 1$ error microphone was considered at $\vartheta_0 = 0$, $\pi/6$ in the downstream half-space. Again, the directivity plots show that the primary sound field is not axially symmetric, and the control performance is degraded as compared to the simplified primary source model of Figs. 2 and 3.

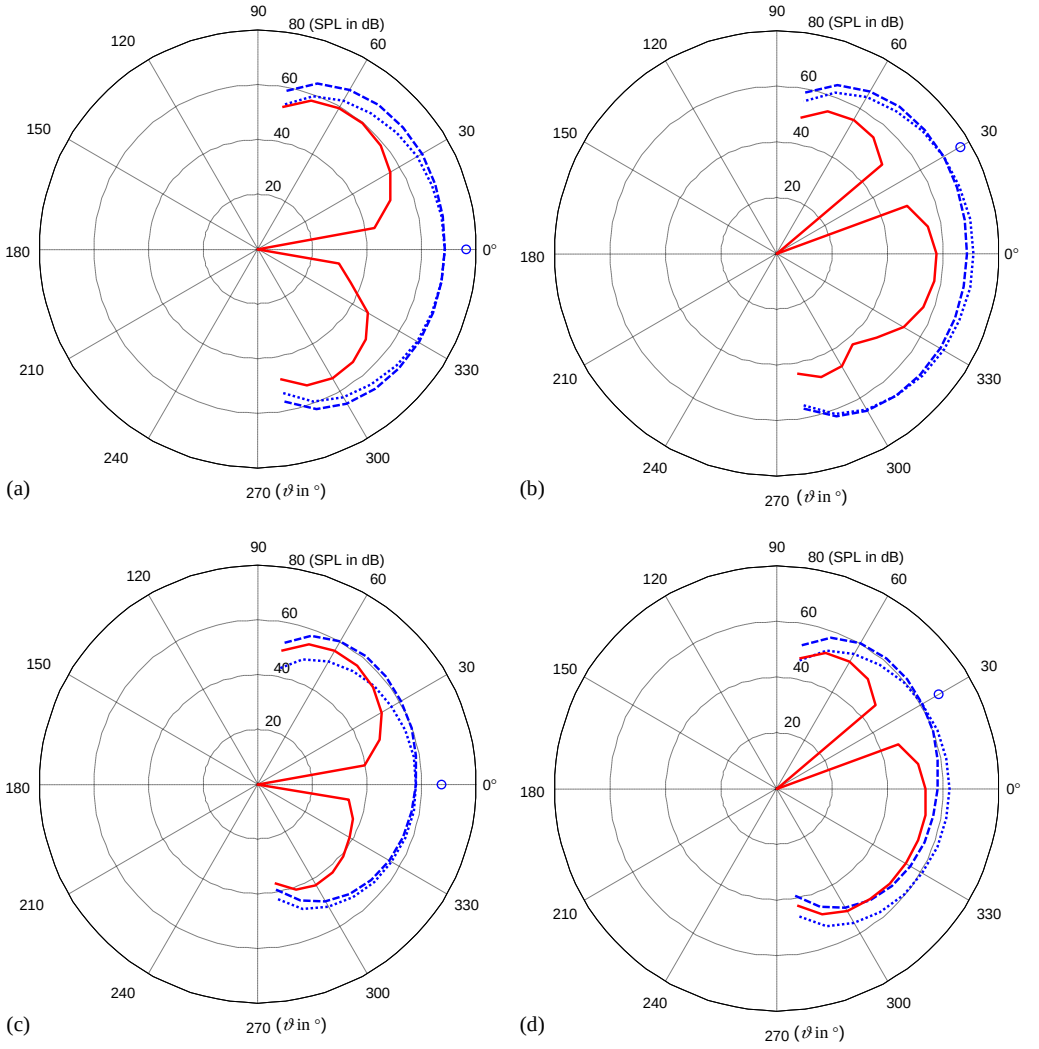

Fig. 9. Primary source (dashed), secondary source (dotted) and resulting field (solid) downstream directivity from the inverse aeroacoustic primary source model, six-bladed fan with equal blade pitches; $a = 4\,\text{cm}$ and $z_s = 5\,\text{cm}$; (a) $\vartheta_0 = 0$, $f = 300\,\text{Hz}$, (b) $\vartheta_0 = \pi/4$, $f = 300\,\text{Hz}$, (c) $\vartheta_0 = 0$, $f = 600\,\text{Hz}$, (d) $\vartheta_0 = \pi/4$, $f = 600\,\text{Hz}$.

However, trends are similar and the control is still global in the downstream half-space with only one cancellation point and one secondary source. For the BPF, the simulated sound power reductions are -11.1 and $-12.0\,\text{dB}$ when the error microphone are located at $\vartheta = 0$ and $\vartheta = \pi/6$, respectively. As far as 2 BPF is concerned, the reductions are -13.9 and $-14.1\,\text{dB}$ for $\vartheta = 0$ and $\vartheta = \pi/6$, respectively. However, one has to remark that those simulated sound power attenuations cannot be achieved experimentally since the reduction of tonal noise is limited by the broadband noise. The accuracy of the attenuation is also limited by the quality of the extrapolated primary sound field directivity. The more dispersed the measured acoustic pressures are, the more complicated the reconstruction is, it can therefore deteriorate the simulated active noise control attenuations.

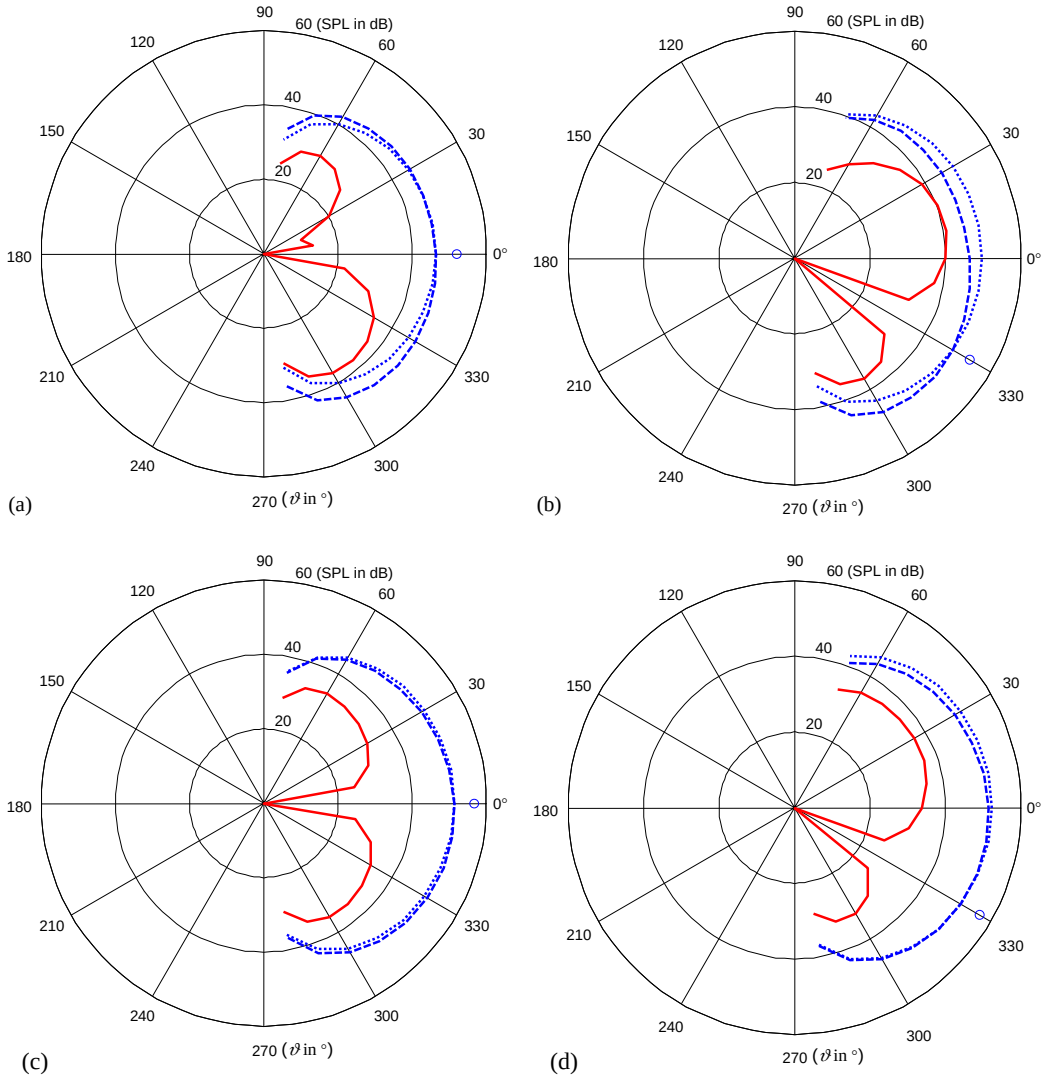

Fig. 10. Primary source (dashed), secondary source (dotted) and resulting field (solid) downstream directivity from the inverse aeroacoustic primary source model, seven-bladed fan with unequal blade pitches; $a = 4\,\text{cm}$ and $z_s = 5\,\text{cm}$; (a) $\vartheta_0 = 0, f = 340\,\text{Hz}$, (b) $\vartheta_0 = \pi/6, f = 340\,\text{Hz}$, (c) $\vartheta_0 = 0, f = 680\,\text{Hz}$ (d) $\vartheta_0 = \pi/6, f = 680\,\text{Hz}$.

6. Active control experiments

In the previous sections, it has been shown that a single dipole located in front of the fan is theoretically capable of globally reducing the long wavelength tonal noise of the fan in free field. In this section, active noise control experiments in free field are presented. The measured directivities and metrics in the downstream half-space with and without control are compared to the previous predictions.

6.1. Experimental set-up

Experiments were conducted on two engine cooling units consisting of a symmetric six-bladed fan or a non-symmetric seven-bladed fan, a radiator and a condenser. In the experiments with the six-bladed fan, the condenser was removed and a small (4×8 cm) rectangular piece of adhesive tape was bonded on the upstream side of the radiator at about 5 cm from the fan axis in order to enhance the non-uniformity of the incoming flow and therefore increase tonal noise radiation. The unit was driven by a variable DC source (0-20V/0-60A); the rotational speed of the fan could be continuously adjusted by modifying the input voltage. The fan has an exterior diameter of 30 cm and a central hub diameter of 12.5 cm.

A small midrange unbaffled control loudspeaker of 8 cm in diameter was bonded at the centre of the stator, corresponding to the centre of rotation of the fan hub (fixed in the laboratory reference frame). The average distance between the plane of the blades and the loudspeaker membrane was $z_s = 5$ cm. It was verified that the loudspeaker has negligible effect on the downstream flow of the fan; in the reported results, all noise data of the fan alone were measured with the control loudspeaker in place. A SISO adaptive feedforward controller was implemented to drive the control loudspeaker. An infrared optical tachometer was mounted on the fan in order to extract a reference signal containing the relevant frequencies: a small rectangular piece of reflective tape was bonded to the outer rotating rim of the blade in order to provide a rectangular pulse train from the detector circuit placed on a fixed location of the frame. In the case of the six-bladed symmetric fan, 6 pieces of reflective tape were equally distributed on the outer rim, so that the reference signal is a train of rectangular pulses with a period equal to the blade passing frequency. In the case of the seven-bladed fan with unequal blade pitches, the reference signal must be designed to contain multiples of the rotational speed of the fan, with important components at multiples of the BPF: this was achieved by unequally distributing 7 reflective strips on the outer rim.

An error microphone (TMS 1/4″ made by PCB) was placed at 1.5 m from the fan centre in the downstream half-space; the microphone could be moved at various directions ϑ_0 from the fan axis. A windscreen was mounted on the microphone to minimise the effect of flow noise. The physical elements of the feedforward active control set-up are shown in Fig. 11. The set-up was placed in a semi-anechoic room with the fan axis horizontal and at 50 cm above the ground. Twelve centimetre of absorbing material (conasorb F) were placed on the ground under the set-up in order to minimise ground reflections.

Active control simulations for this configuration have shown that global control of the downstream sound field can be obtained up to approximately 700 Hz using a single control source. Given that the rotational speed was fixed to approximately 50 Hz, the experimental objective was therefore a global attenuation of downstream noise at 1 and 2 BPF. A time-domain adaptive filtered-X LMS feedforward controller [15] was implemented under a dSPACE/Simulink real-time control environment. The sampling frequency was set to 3000 Hz, and anti-aliasing and reconstruction low-pass filters were placed at input and output stages of the digital signal processing board. The cut-off frequency of the low-pass filters was set to 800 Hz in the case of the six-bladed fan and 1200 Hz in the case of the seven-bladed fan. The secondary path (transfer function between loudspeaker input and error microphone output) was identified off-line by feeding a broadband noise to the secondary source and using an adaptive LMS identification with

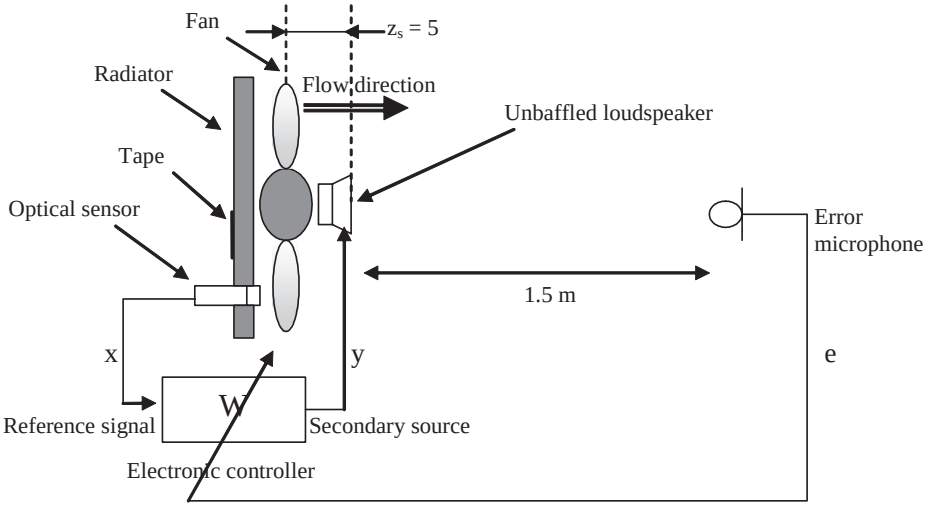

Fig. 11. Physical elements of the single channel feedforward active control of free-field fan.

a 64-tap FIR filter. The control filter was implemented as an FIR filter with 4 coefficients (six-bladed symmetric fan) or 32 coefficients (seven-bladed non-symmetric fan). The measured coherence between the reference sensor and the error microphone at 1 and 2 BPF was larger than 0.98 in all experiments conducted.

At last, a HP 35665A spectrum analyser was used to measure the power spectrums (20 averages for each measurement) at 17 regularly spaced points on a circular arc at 1.5 m from the fan centre, with $\varphi = 0$ and $-80^\circ < \vartheta < 80^\circ$ in the downstream half-space to evaluate the directivity of the primary (without control) and the resulting radiated (with control) sound field.

6.2. *Experimental results on six-bladed fan with equal blade pitches*

The rotational speed of the fan was adjusted to $\Omega = 50$ Hz so that the first 2 disturbing tones are at 1 BPF = 300 Hz and 2 BPF = 600 Hz. Fig. 12 shows the power spectrum of the sound pressure measured at the error microphone location ($\vartheta_0 = 0$) with and without active control. The tones at 1 BPF (300 Hz) and 2 BPF (600 Hz) are decreased by 28 and 18 dB, respectively at the error microphone location, and the residual sound field at these frequencies is essentially the broadband, uncorrelated noise. The size of the control filter (4 coefficients) and the low-pass filtering under 800 Hz leave the tone at 3 BPF unchanged by the control.

The measured directivity without and with active control is shown in Fig. 13. When the error microphone is located on the fan axis ($\vartheta_0 = 0$), the directivity pattern after control is typical of a quadrupole radiation and the tonal noise is globally reduced. Very good agreement between predicted and measured residual sound field is obtained at 1 BPF. Note that the predicted residual sound field has been limited in the following figures to the frequency band of the broadband noise. The agreement is not as good at 2 BPF because of the less-precise reconstruction of the primary sound field of the fan by the inverse method at this frequency [1].

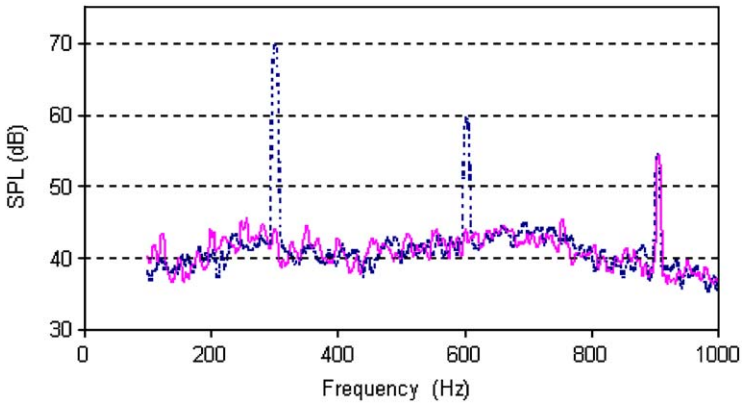

Fig. 12. Power spectrum of the sound pressure at the error sensor position ($\vartheta_0 = 0$) for a six-bladed (with equal pitches) automotive fan noise, with (solid line) and without (dashed line) active control.

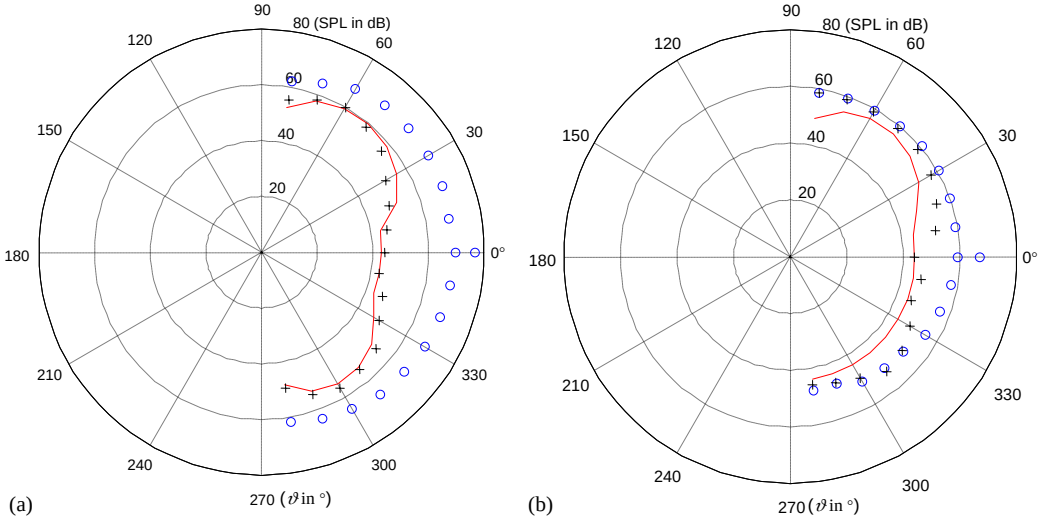

Fig. 13. Measured downstream directivity of a six-bladed (with equal pitches) automotive fan noise at (a) 1 BPF and (b) 2 BPF. Without control (o), with control (+), predicted resulting sound field (solid line). Error microphone at $\vartheta_0 = 0$.

We can have an idea of the sound power reduction from the measured radiation directivity by using the modified half-space sound power parameter $10 \log \eta_W^{\text{half}}$ described in Section 4.2. The reductions calculated from the simplified fan noise model, from the inverse aeroacoustic model of the fan and the measurements are compared in Table 1.

As already shown in Fig. 13, the agreement between measured attenuation in the downstream half-space attenuations and from the inverse aeroacoustic model is very good for 1 BPF, whereas there is a difference of 3.3 dB for 2 BPF. But, it can be seen that the sound power reduction

Table 1
Comparison between the predicted sound power attenuation ($10\log\eta_W^{\text{half}}$) and the experimental directivity measurements for the BPF and its first harmonic (six-bladed fan)

Frequency	From the simplified fan noise model (dB)	From the inverse aeroacoustic model (dB)	Experimental measurements (dB)
1 BPF (300 Hz)	−19.8	−10.8	−10.8
2 BPF (600 Hz)	−11.1	−4.8	−1.5

estimated from the inverse model is more accurate than the reduction estimated from the simplified fan noise model for that case.

6.3. Experimental results on seven-bladed fan with unequal blade pitches

In the case of the non-symmetric fan, the rotational speed of the fan was adjusted to $\Omega = 48.5$ Hz so that the first two disturbing tones are approximately at $1\,\text{BPF} = 340$ Hz and $2\,\text{BPF} = 680$ Hz. Fig. 14 shows the power spectrum of the sound pressure level at the error microphone location ($\vartheta_0 = 0$) with and without active control. The irregular blade spacing has the effect of spreading the acoustic energy over all integer multiples of the rotational speed. The tones at 1 and 2 BPF are still dominant, however their level is lower than for the fan with equal blade pitches. The reference signal in this case is a pulse train with a fundamental period equal to the rotation period of the fan and therefore contains multiple harmonics of the rotation speed. The active control mainly reduces the most energetic peaks at 1 BPF (340 Hz) and 2 BPF (680 Hz) and has a moderate effect on other multiples of the rotational speed of the fan.

Fig. 15 shows the acoustic directivity with and without active control when the error microphone is at $\vartheta_0 = 0$. The 2 tones at 1 and 2 BPF are globally reduced after control and the radiation pattern is once again representative of a quadrupole. The agreement between the measured and predicted sound field after control is reasonably good.

Figs. 16 and 17 show additional results for an error microphone located at $\vartheta_0 = \pi/6$. Again, an effective global control of the tones at 1 and 2 BPF are obtained in this configuration, with a satisfactory directivity agreement between experimental and theoretical control results. As done for the six-bladed fan with equal blade pitches, the reductions calculated from the simplified fan noise model, from the inverse aeroacoustic model of the fan and the measurements are compared in Table 2.

The predicted sound power reductions using the inverse model are overestimated and are not as good as for the six-bladed fan. This can be explained by the different loading conditions between the two experiments and also by the fact that the first BPF directivity is sparse and not well defined, hence the primary sound field is difficult to extrapolate. But the predicted attenuations are still better when using the primary sound field from the inverse model, at least for 1 BPF. Since the directivity of 2 BPF is quasi-dipolar, the modelled resulting radiation using the simplified model give similar results as those obtained using the inverse model.

However, the control is still global in the downstream half-space and no differences are to be noted in the sound power reduction for $\vartheta_0 = 0$ and $\vartheta_0 = \pi/6$.

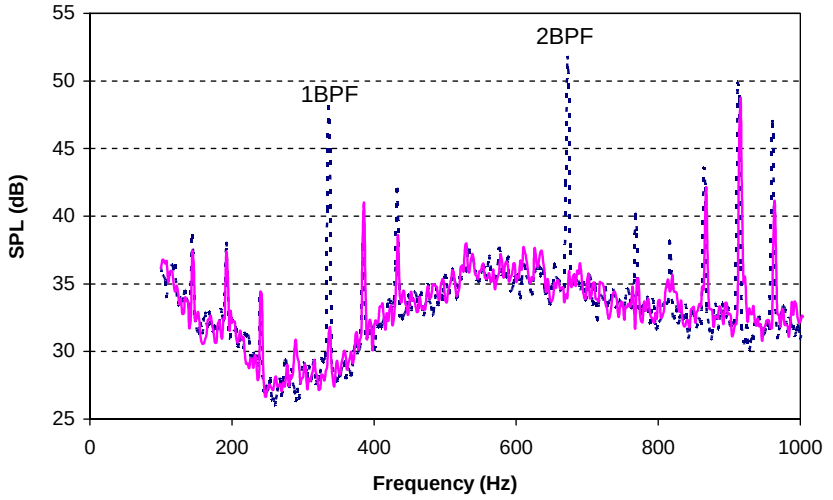

Fig. 14. Power spectrum of the sound pressure at the error sensor position ($\vartheta_0 = 0$) for a seven-bladed (with unequal pitches) automotive fan noise, with (solid line) and without (dashed line) active control.

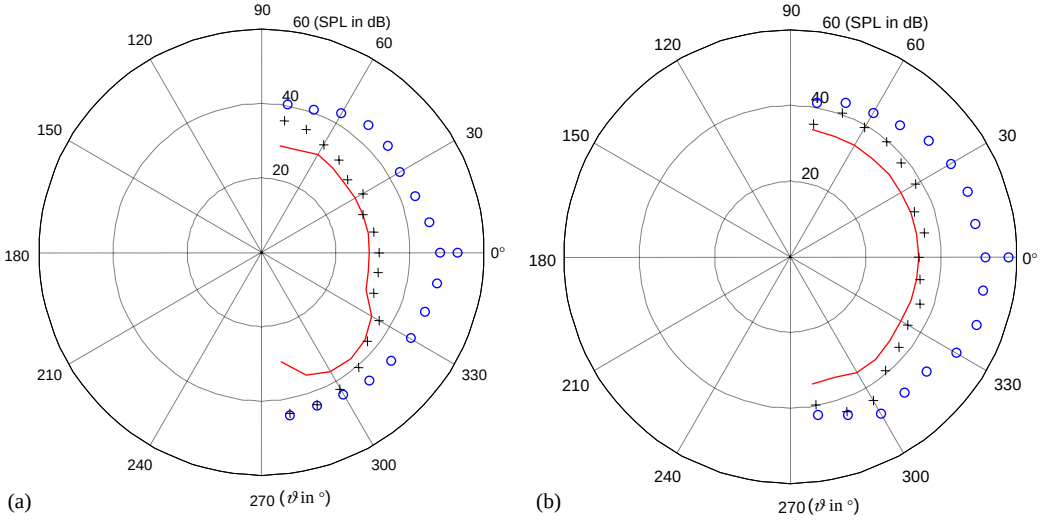

Fig. 15. Measured downstream directivity of a seven-bladed (with unequal pitches) automotive fan noise at (a) 1 BPF and (b) 2 BPF. Without control (o), with control (+), predicted resulting sound field (solid line). Error microphone at $\vartheta_0 = 0$.

7. Conclusion

A model for the fan noise valid only when the most radiating modal component of the flow is taken into account was first derived and combined with a model for loudspeaker radiation to demonstrate the ability of a single loudspeaker located at the front of the fan to attenuate

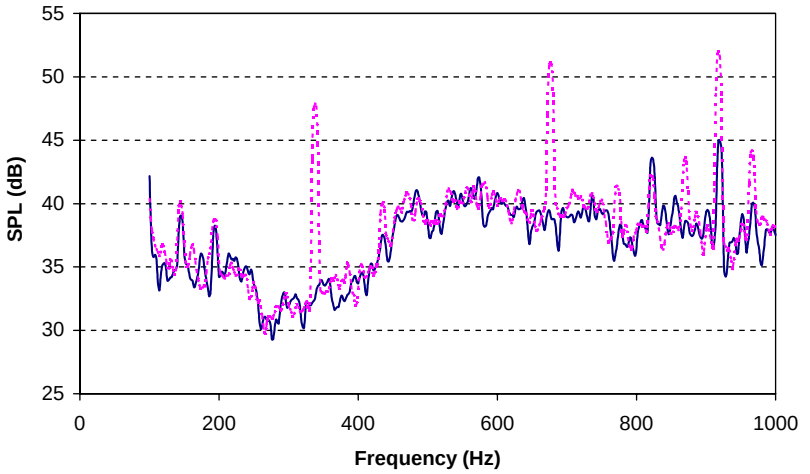

Fig. 16. Power spectrum of the sound pressure at the error sensor position ($\vartheta_0 = \pi/6$) for a seven-bladed (with unequal pitches) automotive fan noise, with (solid line) and without (dashed line) active control.

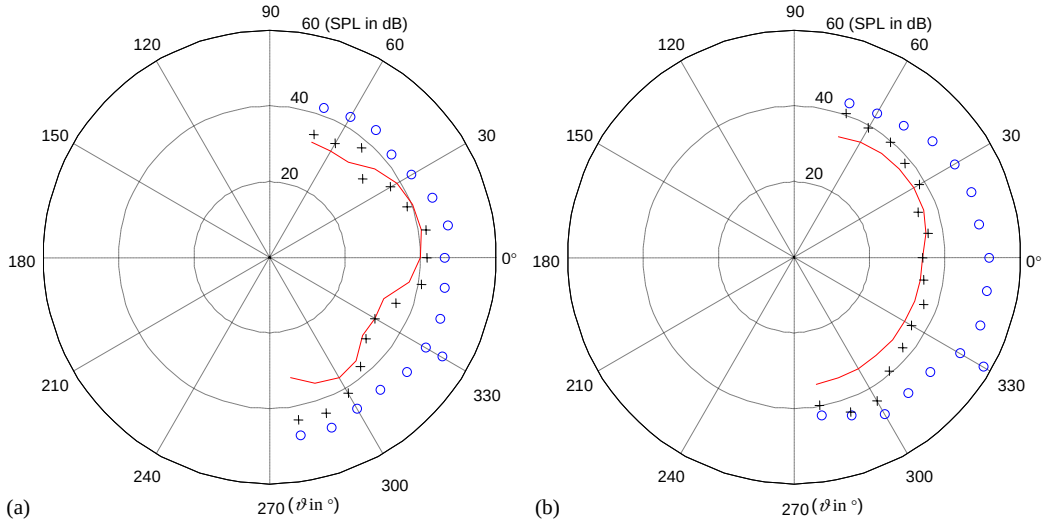

Fig. 17. Measured downstream directivity of a seven-bladed (with unequal pitches) automotive fan noise at (a) 1 BPF and (b) 2 BPF. Without control (o), with control (+), predicted resulting sound field (solid). Error microphone at $\vartheta_0 = \pi/6$.

the free-field radiation in the whole space or in a single half-space as a function of the geometrical features of the primary and secondary source as well as the distance between them. The performance of the approach was evaluated using three metrics for global control. A more detailed model for fan radiation was then presented and used to perform control simulations under non-homogeneous flow conditions. This direct-inverse aeroacoustic model was used to calculate the equivalent sources of a propeller for a non-homogeneous stationary flow field.

Table 2
Comparison between the predicted sound power attenuation ($10\log\eta_W^{\text{half}}$) and the experimental directivity measurements for the BPF and its first harmonic (seven-bladed fan)

Frequency	Simplified fan noise model (dB)	Inverse aeroacoustic model (dB)	Experimental measurements (dB)
1 BPF (300 Hz)			
$\vartheta = 0$	−18.5	−11.1	−5
$\vartheta = \pi/6$	−21.8	−12.1	−5
2 BPF (600 Hz)			
$\vartheta = 0$	−9.1	−11.9	−7
$\vartheta = \pi/6$	−13.4	−13.8	−7

Simulation results making use of the equivalent sources given by the inverse aeroacoustic model were relevant to predict the resulting sound field for long wavelengths. Tonal sound was significantly reduced to the level of the broadband noise at the error microphone location and a global control in the downstream half-space was achieved.

The experimental results clearly demonstrated the ability of the active control system to significantly attenuate the blade passing frequency and its first harmonic (up to 28 dB) in free field. The amount of reduction achieved at the second and higher harmonics of the BPF greatly depends on the location of the error sensor because of the multi-lobed directivities. But, as the noise levels are lower at these higher frequencies, this is not really detrimental; moreover, the attenuation of these frequencies can be achieved passively. The use of a SISO feedforward controller with a filtered-X LMS algorithm also leads to robust adaptive control, and the location of the error microphone is almost a free choice if the loudspeaker is located at the front of the fan. The best arrangement from an active fan noise control point of view is the use of a symmetrical propeller because of the fewer number of harmonics to be controlled and easier measurement of the reference signal. Moreover, the better the primary and secondary source directivities are in agreement, the better the control is. As the secondary source is dipolar, the best control should be achieved at low frequencies and when the fan presents almost axially symmetric patterns.

Future work involves implementing this active noise control system in a vehicle and to investigate an alternative technique to sense the error signal in rugged automotive conditions. The boundary conditions will not be the same but preliminary results shows the feasibility of an "at the source" active control of tonal noise. Future experimental work on the control of the BPF and its harmonics in the whole free space using more than one error microphone will also be conducted to completely assess the simulations in free field.

Acknowledgments

This work has been supported by the AUTO21 Network of Centres of Excellence and Siemens VDO Automotive Inc. The authors wish to thank Sylvain Nadeau from Siemens VDO Automotive Inc. for his collaboration to this research. The authors also thank Dr. Yann Pasco for his contribution to the experimental active noise control.

References

[1] A. Gérard, A. Berry, P. Masson, Control of tonal noise from subsonic axial fan. Part 1: active control simulations and experiments in free field, *Journal of Sound and Vibration*, in press, this issue; doi:10.1016/j.jsv.2005.01.023.
[2] P.A. Nelson, S. Elliot, *Active Control of Sound*, London Academic Press, 1992.
[3] Y.N. Yeung, P. Yu, W.K. Chow, Active noise control: evaluation in ventilation systems, *Building Services Engineering Research and Technology* 17 (4) (1996) 191–198.
[4] L.J. Eriksson, M.C. Allie, C.D. Bremigan, J.A. Gilbert, Active noise control and specifications for fan noise problems, *Proceedings of Noise Con 88*, Purdue University, USA, 1988.
[5] T.M. Kostek, Combining adaptive-passive and fully active noise control in ducts, *Proceedings of the ASME Noise Control and Acoustics Division*, 1997.
[6] Y.J. Wong, Active control of fan noise in a duct, *Proceedings of Active 2002*, Southampton, UK, 2002.
[7] P. Joseph, P.A. Nelson, M.J. Fisher, Active control of fan tones radiated from turbofan engines. I. External error sensors. II. Induct error sensors, *Journal of the Acoustical Society of America* 106 (2) (1999) 766–786.
[8] R.H. Thomas, R.A. Burdisso, C.R. Fuller, W.F. O'Brien, Active Control of fan noise from a turbofan engine, *AIAA Journal* 32 (1) (1994) 23–30.
[9] S. Myers, S. Fleeter, Dipole active control of wake-blade row interaction noise, *Journal of Propulsion* 15 (1) (1999) 31–37.
[10] N.M. Rao, F. Jinwei, R.A. Burdisso, W.F. Ng, Experimental demonstration of active flow control to reduce unsteady stator-rotor interaction, *AIAA Journal* 39 (3) (2001) 458–464.
[11] K.A. Kousen, J.M. Verdon, Active control of wake/blade-row interaction noise, *AIAA Journal* 32 (10) (1994) 1953–1960.
[12] G.C. Lauchle, J.R. MacGillivray, D.C. Swanson, Active control of axial flow fan noise, *Journal of the Acoustical Society of America* 101 (1) (1997) 341–349.
[13] D.A. Quinlan, Application of active control to axial flow fans, *Noise Control Engineering Journal* 39 (3) (1992) 95–101.
[14] P.M. Morse, K.U. Ingard, *Theoretical Acoustics*, Princeton University Press, Princeton, 1986.
[15] S. Elliot, *Signal Processing for Active Control*, Academic Press, London, 2001.
[16] A. Gérard, A. Berry, P. Masson, Active control of automotive fan noise, *Proceedings of Fan Noise 2003*, Senlis, France, 2003.
[17] M.V. Lowson, Theoretical analysis of compressor noise, *Journal of the Acoustical Society of America* 47 (1) (1970) 371–384.
[18] C. Yu, X.D. Li, Feedforward control study on gust/cascade interaction noise, *Acta Aeronautica et Astronautica Sinica* 24 (3) (2003) 237–241 (in Chinese).